REPORT DOCUMENTATION PAGE

Form Approved OMB NO. 0704-0188

1. AGENCY USE ONLY (Leave Blank)	2. REPORT DATE:	3. REPORT TYPE AND DATES COVERED Final Report 1-Aug-2002 - 31-Jul-2005

4. TITLE AND SUBTITLE
Defect Engineering Through Substrate Design

5. FUNDING NUMBERS
DAAD190210305

6. AUTHORS
Thomas F. Kuech, Susan E. Babcock

8. PERFORMING ORGANIZATION REPORT NUMBER

7. PERFORMING ORGANIZATION NAMES AND ADDRESSES
University of Wisconsin - Madison
Research and Sponsored Programs
750 University Ave., 4th Fl.
Madison, WI 53706 -1490

9. SPONSORING/MONITORING AGENCY NAME(S) AND ADDRESS(ES)

U.S. Army Research Office
P.O. Box 12211
Research Triangle Park, NC 27709-2211

10. SPONSORING / MONITORING AGENCY REPORT NUMBER

44037-MS.3

11. SUPPLEMENTARY NOTES
The views, opinions and/or findings contained in this report are those of the author(s) and should not contrued as an official Department of the Army position, policy or decision, unless so designated by other documentation.

12. DISTRIBUTION AVAILIBILITY STATEMENT
Approved for Public Release; Distribution Unlimited

12b. DISTRIBUTION CODE

13. ABSTRACT (Maximum 200 words)

The abstract is below since many authors do not follow the 200 word limit

14. SUBJECT TERMS
Defect Engineering, narrow gap semiconductors, lateral epitaxial overgrowth

15. NUMBER OF PAGES
Unknown due to possible attachments

16. PRICE CODE

17. SECURITY CLASSIFICATION OF REPORT	18. SECURITY CLASSIFICATION ON THIS PAGE	19. SECURITY CLASSIFICATION OF ABSTRACT	20. LIMITATION OF ABSTRACT
UNCLASSIFIED	UNCLASSIFIED	UNCLASSIFIED	UL

Report Title

Defect Engineering through Substrate Design

ABSTRACT

A comprehensive program in the control of extended defects associated with the growth of large lattice-mismatched materials was undertaken. This program was aimed at understanding the interaction of extended defects with stress that is intentionally introduced into a substrate structure and develop processes for the growth of large lattice mismatched materials with a substantially reduced defect density over large substrate areas. The narrow band gap semiconductors, GaSb and InAs, were used in these studies. TThe application of a lateral epitaxial growth technique (LEO) led to a dramatic and unexpected reduction in defect density when the mask openings are restricted to less than 1 μm. Our measurements indicate an appropriately engineered substrate can lead to dramatic changes in the defect structure leading to the isolation of lattice-mismatched based dislocations to the interface region leading to strong reduction in the dislocation density in the overlying layers. A detailed characterization of the defect structure demonstrated defect reduction in the LEO substrates.

List of papers submitted or published that acknowledge ARO support during this reporting period. List the papers, including journal references, in the following categories:

(a) Papers published in peer-reviewed journals (N/A for none)

1. " Lateral epitaxial overgrowth of InAs on (100) GaAs substrates", G. Suryanarayanan, A.A. Khandekar, B.E. Hawkins, T.F. Kuech, S.E. Babcock, Progress in Semiconductors II - Electronic and Optoelectronic Applications, Mater. Res. Soc. Symposium Proceedings Vol.744), 2003, p 9-14.
2. " Microstructure of lateral epitaxial overgrown InAs on (100) GaAs substrates", G. Suryanarayanan, A.A. Khandekar, T.F. Kuech, S.E. Babcock, Appl. Phys. Lett. 83 (2003) 1977-9.
3. "A comparative study of GaSb (100) surface passivation by aqueous and nonaqueous solutions", Z. Y. Liu, T. F. Kuech, D.A. Saulys, Appl. Phys. Lett. 83 (2003) 2587-9.
4. "Chemical and structural characterization of GaSb(100) surfaces treated by HCl-based solutions and annealed in vacuum", Z. Y. Liu, B. Hawkins, and T. F. Kuech, J. Vac. Sci. Technol. B21 (2003) 71-77.
5. "Effects of Gas switching sequences on GaAs/GaAs1?ySby superlattices, B.E. Hawkins, A.A. Khandekar, J.Y. Yeh, L.J. Mawst and T.F. Kuech, J. Crystal Growth 272 (2004) 686-693.
6. "Modifications of the electronic structure of GaSb surface by chalcogen atoms: S, Se, and Te", Z. Y. Liu, A. A. Gokhale, M. Mavrikakis, D. A. Saulys, and T. F. Kuech, J. Appl. Phys. 96, 4302-7 (2004).
7. "Improved characteristics for Au/n-GaSb Schottky contacts through the use of a nonaqueous sulfide-based passivation", Z.Y. Liu, D.A. Saulys, T.F. Kuech, Appl. Phys. Lett. 85 (2004) 4391-3.
8. "Photoluminescence studies on Al and Ga interdiffusion across (Al,Ga)Sb/GaSb quantum well interfaces", M. Gonzalez-Debs, J.G. Cederberg, R.M. Biefeld, T.F. Kuech, J. Appl. Phys. 97 (2005) 103522-1-8.

Number of Papers published in peer-reviewed journals: 8.00

(b) Papers published in non-peer-reviewed journals or in conference proceedings (N/A for none)

Number of Papers published in non peer-reviewed journals: 0.00

(c) Papers presented at meetings, but not published in conference proceedings (N/A for none)

1. "Lateral Epitaxial Growth Overgrowth of InAs on GaAs Substrates", A. Khandekar, Dept of Chemical Engineering, S. Ganesan, Materials Science Program, B. Hawkins, Dept of Chemical Engineering, S.E. Babcock, Dept Materials Science and Engineering, T.F. Kuech, Materials Research Symposium Meeting, Boston, MA, November, 2002.
2. "Characterization and Structural Analysis of MOCVD-grown InAs Thin Films on (100) GaAs", A Khandekar, G. Suryanarayanan, S. Babcock, T. Kuech, Amer. Conf. on Crystal Growth, Keystone, CO, July 20-24, 2003. "Microstructure of Lateral Epitaxially Overgrown InAs Thin Films:", G. Suryanarayanan; A. A. Khandekar; T. F. Kuech; S. E. Babcock, Electronic Materials Conference, Salt Lake City, Utah, June 25-27,2003.
3. "Interdiffusion Studies of Al and Ga in AlSb/GaSb Quantum Wells", M. Gonzalez Debs, J. G. Cederberg, R. M. Biefeld, T. F. Kuech, Electronic Materials Conference, Salt Lake City, Utah, June 25-27, 2003.
4. (Invited) "Heterogeneous Materials and Devices Integration: from Substrate Technology to Active packaging", April S. Brown, Nan Marie Jokerst, Thomas F. Kuech, Materials Research Symposium Meeting, San Francisco, CA, April 21-25, 2003.
5. (Invited) "Materials Integration in Micro- and Opto-electronics", T.F. Kuech, Stine Award Lecture, American Institute of Chemical Engineering Conf., San Francisco, CA, Nov. 16-16, 2003.
6. (Invited) "Mask-Pattern-Dimensions Induced Changes in Microstructural Development During LEO: InAs on GaAs with Sub-Micron Windows," S.E.Babcock, G. Suryanarayanan, A.A. Khandekar, and T.F. Kuech, International Conference on Alternative Substrate Techologies, Chamonoix, France, March 2004.
7. "Development of Crystal Tilt During Early Stages of MOCVD Growth of InAs on (100) GaAs as Revealed by Electron Backscatter Diffraction," G. Suryanarayanan, A.A. Khandekar, T.F. Kuech, S.E. Babcock, International Conference on MOCVD, Maui, June 2004
8. "Extended Defect Microstructure of Metamorphic Buffer Layers based on AlGaSb and InAsP", G. Suryanarayanan, A.A. Khandekar, T.F. Kuech, S.E. Babcock, P.W. Deelmand, R.D. Rajaveld, K. Elliott, D.H. Chow, 46th Electronic Materials Conference, Notre Dame, IN from June 23-35, 2004.
9. "Modifications of GaSb surface electronic structure by the Chalcogen atoms: S, Se and Te", Zhiyan Liu, Amit Gokhale, Manos Mavrikakis, Thomas F. Kuech, 46th Electronic Materials Conference, Notre Dame, IN from June 23-35, 2004.
10. "Effects of Gas Switching Sequences on the Structure of GaAs/GaAsSb Superlattices grown by MOVPE", B. E. Hawkins, A. A. Khandekar, J. Y. Yeh, L. J. Mawst, T. F. Kuech, International Conference on Metal Organic Vapor Phase Epitaxy, Maui, HA, May 30-June 4, 2004.
11. "Tilted Origin of Multiply-Tilted Grains in Conventional and Lateral Epitaxial Overgrowth of InAs Thin Films on (100) GaAs by MOCVD", A.A. Khandekar, G. Suryanarayanan, S.E. Babcock, and T.F. Kuech, 46th Electronic Materials Conference, Notre Dame, IN from June 23-35, 2004.
12. "Control of Crystal Tilt in MOCVD Films of InAs on (100) GaAs", S.E. Babcock, A. Khandekar, T.F. Kuech, G. Suryanarayanan, Materials Research Society Meeting, Boston, Nov. 30 –Dec. 2, 2004. "Lateral Growth Behavior of GaSb by Metal Organic Vapor Phase Epitaxy", B. E. Hawkins and T. F. Kuech, 46th Electronic Materials Conference, Notre Dame, IN from June 23-35, 2004.
13. "Structural Evolution of the Microstructure of InAs on GaAs," A.A. Khandekar, G. Suryanarayanan, S.E. Babcock, T.F. Kuech, International Conference on MOCVD, Maui, June 2004
14. "Development of InAs Defect Microstructure on Patterned (100) GaAs Substrates", G. Suryanarayanan, A.A. Khandekar , T.F. Kuech, S.E. Babcock", G. Suryanarayanan, A.A. Khandekar, T.F. Kuech, S.E. Babcock, International Conference on Crystal Growth, Grenoble, France, Aug. 8-12. 2004.
15. "InAs Growth and the Development of the Defect Microstructure on GaAs," A.A. Khandekar, G. Suryanarayanan, S.E. Babcock, T.F. Kuech, International Conference on Crystal Growth, Grenoble, France, August 2004.
16. "Control of Crystal Tilt in MOCVD Films of InAs on (100) GaAs," G. Suryanarayanan, A.A. Khandekar, T.F. Kuech, S.E. Babcock, 2004 MRS Fall Meeting, November 2004.
17. "GaSb surface electronic structure modification by S, Se and Te", Zhiyan Liu, Amit Gokhale, Manos Mavrikakis, T. F. Kuech, AICHE Meeting, Austin, TX, Nov. 8-11, 2004.
18. (Invited) "Approaches to the formation of regular arrays of submicron GaAs", T. F. Kuech, A. A. Khandekar, J. D. Beach, C. Veauvy, C. Allen, R. T. Collins, R. E. Hollingsworth, Photonics West 2005, San Jose, Jan. 24, 2005.
19. "Density Functional Theory Studies of Al and Ga Diffusion in AlSb/GaSb Structures", M. Gonzalez-Debs, A. A. Gokhale, M. Mavrikakis1; T. F. Kuech, 47th Electronic Materials Conference, Santa Barbara, CA from June 22-34, 2005.
20. "Island Size Distribution in InAs Grown on (100) GaAs by Metalorganic Vapor Phase Epitaxy", A. A. Khandekar, G. Suryanarayanan, J. Webb, M.K. Rathi, S.E. Babcock and T.F. Kuech, ACCGE 16, Big Sky, MT, July 10 - 15, 2005.

Number of Papers not Published: 20.00

(d) Manuscripts

1. "Microstructural and Morphological Investigations of Metalorganic Vapor Phase Epitaxy-grown InAs Thin Films on (100) GaAs", A.A. Khandekar, G. Suryanarayanan, S. E. Babcock, and T. F. Kuech, J. Crystal Growth, submitted 11/05.
2. "Growth Behavior of GaSb by Metal Organic Vapor Phase Epitaxy", M. K. Rathi, B. E. Hawkins and T. F. Kuech, J. Crystal Growth, submitted 11/05.

Number of Manuscripts: 2.00

Number of Inventions:

Graduate Students

Suryanarayanan Ganesan, Ph.D, Materials Science Program Graduate Student (25 months, 12 month internal fellowship))
Mariam Gonzalez-Debs, Ph.D (Granted 2005), Chemical Engineering Graduate Student (5 months)
Brian Hawkins, Ph.D (Granted 2004), Chemical Engineering Graduate Student (materials support, no salary)
Anish Khandekar, Ph.D, Chemical Engineering Graduate Student (15 months)
Zhiyan Liu, Ph.D, (Granted 2004)Chemical Engineering Graduate Student (5 months)
Ning Liu, , Ph.D, Materials Science Program Graduate Student (2 months)

Number of Graduate Students supported: 6.00

Total number of FTE graduate students: 4.00

Names of Post Doctorates

Number of Post Docs supported: 0.00

Total number of FTE Post Doctorates: 0.00

List of faculty supported by the grant that are National Academy Members

Names of Faculty Supported

Susan E. Babcock, Professor, Materials Science and Engineering
Thomas F. Kuech, Professor, Chemical Engineering

Number of Faculty: 2.00

Names of Under Graduate students supported

Number of under graduate students: 0.00

Names of Personnel receiving masters degrees

Number of Masters Awarded: 0.00

Names of personnel receiving PHDs

Mariam Gonzalez-Debs, Ph.D (Granted 2005), Chemical Engineering Graduate Student
Brian Hawkins, Ph.D (Granted 2004), Chemical Engineering Graduate Student
Zhiyan Liu, Ph.D, (Granted 2004)Chemical Engineering Graduate Student

Anish Khandekar, Ph.D, Chemical Engineering Graduate Student (Expected 2006)
Suryanarayanan Ganesan, Ph.D, Materials Science Program Graduate Student (Expected 2006)
Ning Liu, , Ph.D, Materials Science Program Graduate Student (Expecetd 2006)

Number of PHDs awarded: 6.00

Names of other research staff

Sub Contractors (DD882)

Inventions (DD882)

Defect Engineering through Substrate Design

Thomas F. Kuech and Susan E. Babcock

DAAD19-02-1-0305
Final Report : August 1, 2002 through July 31, 2005

I. Table of Contents

II. List of Illustrations and Tables

III. Statement of the Problem Studied

The integration of large lattice mismatched materials onto a substrate of a differing lattice parameter is complicated by the generation of a high density of extended defects. The underlying technology need is materials integration: the monolithic or polylithic assembly of functional materials and devices and the generation of device structures for which no lattice-matched substrate exists. The characterization and understanding of the transition between stages of strain relaxation, passing from pseudomorphic growth through island formation and finally film coalescence, is required to control the extended defect structure. These stages in strain relief are shown to be dependent on growth temperature, substrate structure and surface stiochiometry.

IV. Summary of the most important results

1. Introduction

The potential for new high-performance devices that is offered by the small band gap arsenide and antimonide semiconductors[1,2], together with the current lack of commercially-produced semi-insulating substrates that are lattice matched to these materials, has stimulated renewed interest in heteroepitaxy of cubic compound semiconductors on GaAs and InP. The rate of development of such device structures on GaAs has been moderated, however, by the approximately 7% lattice mismatch between the "6.1 Å" materials (GaSb, InAs, InSb) and GaAs. This large mismatch generally translates to high defect densities and complex microstructures when these materials are grown directly on as-received GaAs wafers using standard growth techniques. The lateral epitaxial overgrowth (LEO) approach has proven to yield defect reduction and affect the threading dislocation microstructure in GaSb/GaAs[3] and in other lattice mismatched systems, such as GaN/Al_2O_3.[4-6] This project investigated application of the LEO technique to the InAs/GaAs heteroepitaxial system. A series of coupled studies of the development of island size, morphology and microstructure during the island stage of grown that was performed in this project provided insight in to the mechanisms by the defect microstructure develops in islands, films and LEO material.

In LEO, a single-crystal substrate is coated with an amorphous masking material, into which openings (windows) are patterned. Material that is later grown on the patterned substrate nucleates on the crystalline material that is exposed in the windows and subsequently grows laterally over the amorphous mask until it coalesces into a continuous film. A reduction in the density of mismatch-derived defects is anticipated because much of the epitaxial film is not in direct contact with a lattice mismatched crystalline substrate. Such defect reduction has, in fact been realized in several heteroepitaxial systems. Though the details are substantially different, the experiments performed as part of this study show that, like in the case of GaN/Al_2O_3, the defect control that can be achieved by LEO is both greater and more complex in its detail than a simple blocking affect by the mask would yield.

Key advances of two general types were achieved. First, this work showed that that LEO can be used to control the defect microstructure in InAs/GaAs and identified growth and substrate conditions that lead to dramatic improvements in the crystal quality of the film. Second, and we believe much more far reaching in its implications, it revealed important steps in the film growth process that lead to defect formation, thereby providing underpinning knowledge for more general defect control in heteroepitaxy that occurs by island growth.

2. Experimental Methods

2A. MOVPE Growth

All InAs epilayers were deposited on semi-insulating (SI) (100) GaAs substrates using metal organic vapor phase epitaxy (MOVPE) with trimethyl indium and arsine as the precursors. GaAs epi-ready wafers with either a 0° or a 2° miscut towards $[1\bar{1}0]$ were used as the substrates. Prior to deposition the substrates were annealed at the growth temperature for 5 minutes in arsine to desorb native surface oxides. A 100 nm thick homoepitaxial layer of GaAs was deposited using trimethyl gallium and arsine at 700°C and a V/III ratio of 100 prior to the InAs deposition. All InAs deposition was carried out at a nominal growth rate of 0.07 μm/min.

The effects of growth temperature, V/III ratio, and deposition time on the microstructural evolution of the InAs islands and films on mask-free substrates were determined prior to investigating the effects of the LEO. In one set of experiments, InAs was grown on unmasked substrates at growth temperatures of 500, 600 and 700°C with a V/III ratio of 80. In a second set, InAs was grown with V/III ratios of 2, 10 and 80 at a constant growth temperature of 700°C. For each growth condition in the above two sets, growth times of 12 seconds and 20 minutes were used to give rise to uncoalesced islands and a 1.4μm thick coalesced InAs film, respectively. In a third set of experiments, growth times from 4 seconds to 2.5 hours at V/III ratio of 80 and growth temperature of 700°C were examined in order to evaluate the evolution of the microstructure during growth.

2B. Island Stage Growths.

A substantial portion of the research concentrated on study of the evolution of microstructure during the island growth stage, prior to coalescence. InAs islands were grown at 700°C and a V/III ratio of 80 for equivalent calibrated thicknesses of (i) 14 nm, (ii) 70 nm and (iii) 210 nm. At each of these stages of growth, investigations of the microstructure showed that the lattice-mismatch derived strain leads to a Stranski-Krastanov growth mode characterized by the formation of coherent three-dimensional InAs islands after the layer-by-layer deposition of just a few monolayers.[3] At every stage of island growth investigated, the InAs islands essentially were all isolated. Coalesced films were grown on as received wafers and LEO substrates using the same reactor conditions to elucidate the role of the island growth stage in establishing the final film microstructure.

The InAs island size distribution was determined for the samples grown for 4 and 12 seconds at 700°C and a V/III ratio of 80 on 0° miscut substrates. The need to determine island sizes over a broad range of sizes with significant statistical precision and, in some cases, of dimensions approaching the detection limits of the AFM necessitated considerable effort in developing robust measuring and analysis methods. The following approach was developed and applied.

Nine AFM scans were obtained from each of the samples at each of four different scan areas: 10x10, 20x20, 40x40 and 60x60 μm^2. Each scan-size exhibits a bias. For example, images recorded at smaller scan sizes are more sensitive to smaller islands but may intersect only segments of larger islands and hence undercount the larger islands of size outside of the spatial bandwidth of the scan. Conversely, larger islands are well represented in larger scans, but smaller islands may remain undetected. The scan areas were selected such that the smallest islands were detected in the smaller area scans and the larger islands were abundantly represented in the larger area scans. The footprint area (μm^2) of each island was extracted from the AFM images using commercial image-analysis software. A cumulative distribution function (CDF) was determined for each scan separately. The CDF is defined as the number of islands per scan area with a footprint area less than or equal to a given value on the absyssa. The determination of the underlying island distribution function is complicated by the resolution limit of AFM at a given scan range. The CDF's were numerically differentiated at each data point using a second order Lagrange's interpolating polynomial for unevenly spaced data. The resulting island number frequency distribution per unit area (IFD) from the four progressively larger scan sizes were compared. Island size ranges were identified where the distributions from two adjacent scan ranges yielded the same island density. The overall distribution was generated by concatenating the distributions from progressively larger scan ranges, matching the distributions over ranges that yielded identical island distributions. The resulting curve is the island size frequency distribution function per unit area over a broad range of experimentally accessible island sizes. This procedure eliminates the inherent bias in the distribution function which can result from the binning of the data into user-defined area windows. As shown in this study, the smallest scan size of 10x10 μm^2 captures the highest number of islands per unit area and was therefore used to estimate the areal island number density for various other growth conditions.

2C. Lateral Epitaxial Overgrowth

Results of application of the lateral epitaxial overgrowth (LEO) method to InAs on GaAs are described in sections 3B and 3D. The LEO substrates used for this part of the research consisted of 0°-miscut (100) GaAs wafers onto which ~120 nm of SiO_2 were deposited by low-pressure chemical vapor deposition. Stripe-shaped windows of width 0.8 μm, 2 μm and 5 μm were etched into the SiO_2 at 10 μm pitch using standard photolithographic and etching techniques. The long axis of the stripes was oriented along the

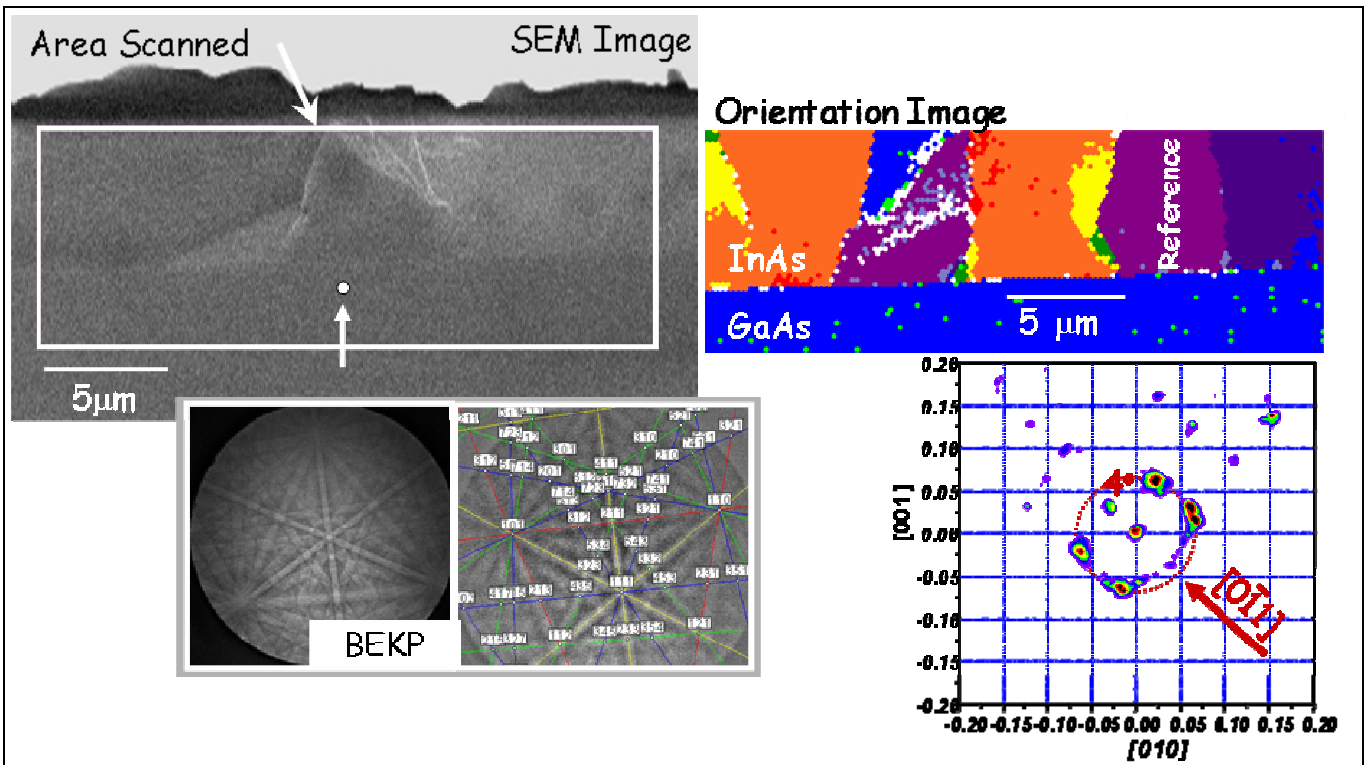

Figure 2A1: Capabilities of BEKP and OIM. Sample is a 7 μm thick film grown at 700°C with a V/III ratio of 80 SEM image is a secondary electron image of an as-fractured cross-sectional surface. BEKP is the pattern collected from one point of the image. Right-hand BEKP shows results of automated indexing of a BEKP pattern. Orientation image is color coded to show the local angle of misorientation relative to a point in the magenta region labeled reference. Pole figure is constructed from orientation measurements made in the scanned area.

$[01\bar{1}]_{GaAs}$. Previous experiments with stripes oriented along the full range of crystallographic directions indicated that the lateral growth rate of the InAs is maximum for stripes oriented along $[01\bar{1}]_{GaAs}$. InAs was grown directly on this GaAs surface. Films were grown to various nominal thicknesses, yielding deposits that ranged from well-isolated islands to thick coalesced films in order to study the evolution of the microstructure and crystal orientation. Each growth run included both LEO and unpatterned (100) GaAs (i.e., control) substrates.

2C. Characterization Techniques

The InAs crystal quality and orientation were characterized through out all of the studies using combinations of double crystal x-ray diffraction (DCXRD) rocking curves, x-ray pole figure analysis ((400) InAs peak), and backscattered electron Kikuchi pattern analysis. Tapping mode atomic force microscopy (AFM) in air was used to characterize the island surface morphology of the short growth time samples and film surface morphology of the long growth time samples. Cross-sectional transmission electron microscopy (TEM) was used to study the defect structure in several samples. TEM samples were prepared using the tripod polishing method with a final ion-milling step.

Application of BEKP analysis and the associated Orientation Imaging Microscopy (OIM) technique is somewhat new to the study of epitaxial films. BEKPs are diffraction patterns produced by backscattered electrons that are generated in SEM experiments. Analysis of the patterns can lead to phase identification data and determination of local crystal orientation with at least 0.5° precision at a spatial resolution of 100 nm. Patterns can be collected with a stationary ("spot mode") or scanning electron beam. In spot mode, the electron beam is positioned at a point of interest in the sample, for example, the dot in the Fig 3A1 and a Kikuchi pattern, also shown in the figure, is collected, stored, and later analyzed. In scanning mode, the electron beam is rastered, for example over the area outlined by the white box in Fig. 2A1. BEKPs are collected and analyzed automatically as the beam scans. Spatial coordinates and Euler angles that describe the location and local orientation of the crystal, respectively, are stored. From these data orientation images, pole figures, and other renditions of the crystal orientations present in the area rastered can be constructed. The colors in orientation images, like that shown in Fig. 3A1, reflect the angle of rotation between the orientation of the phase at that point in the image and a reference orientation. (The crystal rotation between the reference and local orientation is often referred to as the misorientation.) In Fig. 3A1, the reference orientation is the local InAs orientation measured at a point in the magenta region. The InAs reference orientation, chosen at random is misoriented 3-4° relative to the GaAs wafer, and thus the wafer is colored blue in the image. The orientation information from the scanned region can also be displayed as a pole figure specific to that region, also illustrated in Figure 3A1. The orientation imaging power of this technique proved to be an in valuable tool for understanding how the InAs microstructure develops as the film grows and what the mechanism for introduction of the systematic tilt observed in many of the samples might be.

3. Experimental Results

3A. Crystallographic Tilt in InAs Grown on GaAs under Conditions that Favor a Low Nucleation Rate

The crystal quality for continuous films grown on unpatterned substrates at the various combinations of growth temperature and precursor composition was examined using x-ray diffraction methods. X-ray rocking curves and x-ray pole figures like those shown in Figure 3A1 revealed that not only the crystal quality and microstructure, but also the orientational purity of the film are sensitive to the gas-phase stoichiometry and the growth temperature. The (400) InAs pole figure in Fig. 3A1 illustrates most clearly the distribution of orientations that arises in continuous films on unpatterned substrates the higher temperatures and higher V/III ratios. The lack of intensity at the center of the pole figure reveals that in little to none of InAs volume has the InAs [001] aligned with the GaAs [001]. Rather the film is comprised of InAs domains in which the epilayer is tilted by a few degrees relative to the GaAs in one of six different orientations. The x-ray rocking curves shown are consistent with the orientation distribution.

The pole figure reveals clearly that essentially none of the InAs is oriented parallel to the GaAs when the growth temperature is 700°C (no intensity at the middle of the pole figure) and the V/III ratio is 80. Films grown at lower temperature (500°C) and any V/III ratio within the range studied, x-y, have singular orientation as evidence by a single, albeit rather broad for applications in electronics, InAs peak in (400) rocking curves. A strong correlation between growth conditions that favored relatively high nucleation rates and the presence of a single InAs crystal orientation, aligned with the GaAs was observed for the range of growth temperature and growth chemistries investigated. Conversely, conditions predicted to

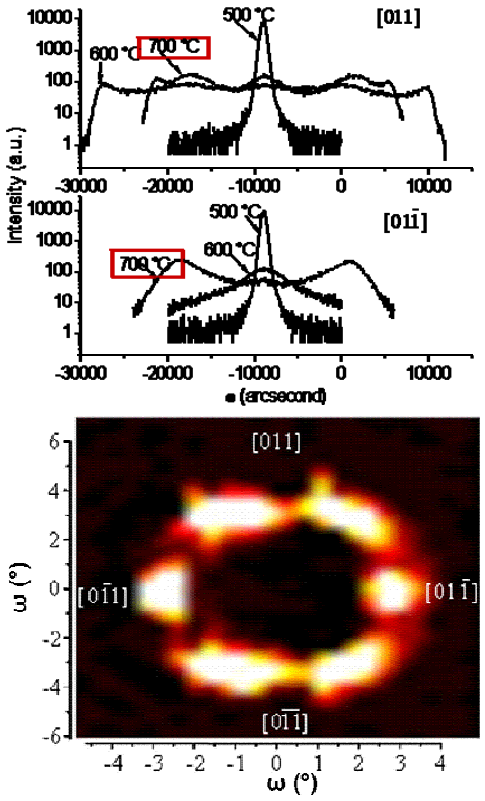

Figure 3A1. X-ray rocking curves as well as the pole figure from InAs films grown on GaAs with no substrate miscut. The pole figure was generated from a film grown at 700°C.

result in a relatively low nucleation rate (higher T, for example) generally resulted in the presence domains of tilted InAs in the film. A singular orientation was obtained at a growth temperature of 700°C and a low V/III=2 which were conditions leading to a high nucleation rate and coalescence at a small island size.

The orientation image in Fig. 2A1 was obtained from a polished cross-section of a film grown at 700°C with a V-III ratio of 80. It shows that the multiple preferred orientations detected in x-ray rocking curves and pole figures originate from columnar grains with mean diameters on the order of a few micrometers. The image also suggests that the tilt is established at or very near the substrate/film interface and then propagates directly through the film. No tendency for significant evolution of the pattern or distribution of tilted material with thickness is suggested by the orientation image. TEM characterization of this film revealed the same microstructural features, albeit with far more demanding experimental methodology. The pole figure shown in Figure 3A1 was generated from the BEKP measurements of local orientation used to generate the OIM in the figure. Comparison of the BEKP pole figure generated from this small volume of the film with the x-ray pole figure in 3A2 that obtained from a much larger area of the film indicates that the essential features of the tilt spectrum in the film are duplicated in micron-scale areas. Subsequent studies of tilt within individual islands, described in Section 3C showed that the tilt microstructure has its origins within individual islands and is thus repeated on the scale of the island size at coalescence. (See section 3C for details.)

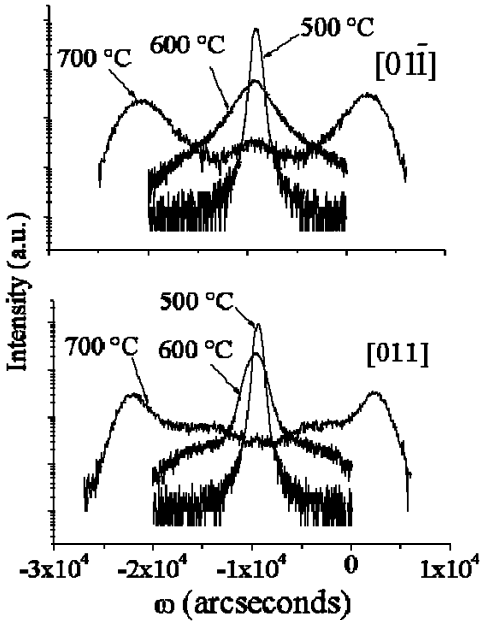

Figure 3A2. X-ray rocking curves as well as the pole figure from InAs films grown on GaAs with 2° miscut.

Figure 3A1 presents InAs (400) x-ray rocking curve scans with ω along the $[011]$ and $[01\bar{1}]$ directions for several films as a function of growth temperature for GaAs substrates having a 0° miscut. A single, narrow rocking curve peak is obtained from the samples grown at 500°C in both the scan directions. The position of this single peak for the 500°C sample corresponds to the InAs (100) planes aligned parallel to the substrate GaAs (100) planes. For the higher growth temperature samples, multiple peaks appear in the rocking curve scans. When multiple peaks are present, the angular difference between the InAs orientations is anisotropic with respect to the two scan directions; larger tilts are observed along $[011]$ scan direction.

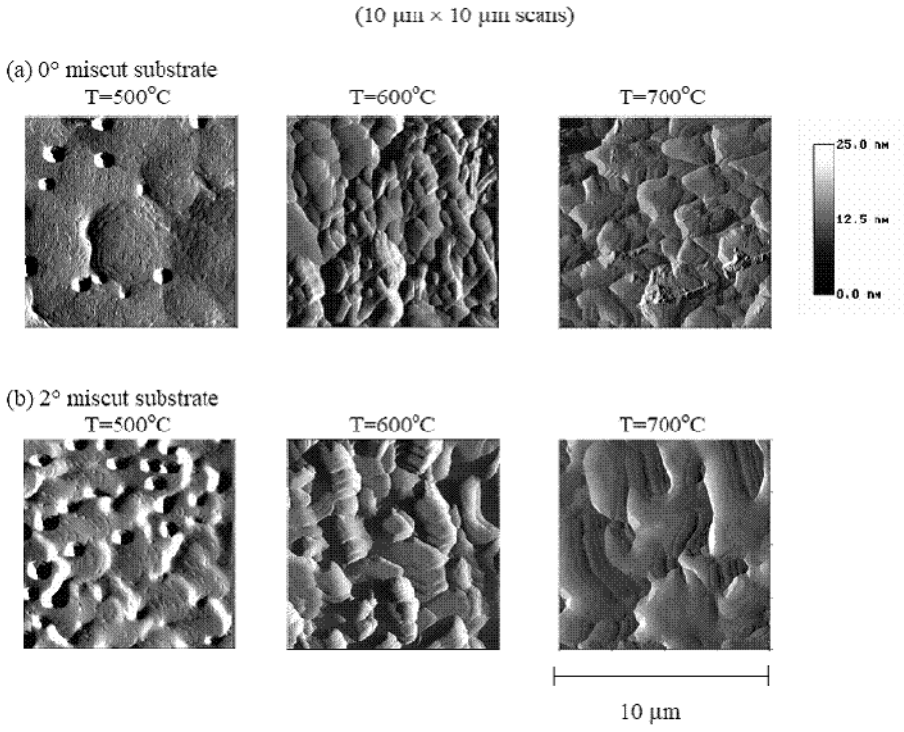

Figure 3A3. AFM amplitude (height derivative) images (10 μm × 10 μm scan size) for samples grown for 20 minutes (InAs thin film) with growth temperature as parameter (constant V/III ratio of 80): samples with a) non-miscut substrate, b) with 2° miscut substrate.

For the samples grown on 2° miscut substrate shown in Figure 3A2, a single peak in obtained in the rocking curve scans for 500 and 600°C growths; multiple peaks are observed for 700°C growth. A set of multiple tilts which are anisotropic with respect to the scan direction is present in the sample grown at 700°C on 2° miscut substrate. An additional difference between InAs growth on the 0° and 2° miscut substrates is that the InAs films grown on the 2° miscut substrates have an overall tilt of InAs (400) peak with respect to GaAs (400) peak by 400 to 600 arcseconds in both scan directions. The multiple tilts are superimposed on this overall tilt, whenever the multiple tilts are present for the InAs film grown on the 2° miscut substrates. The overall tilt was determined by repeating the rocking curve scans of the (400) peak after rotating the sample by 180° about the sample normal and measuring the shift in the peak positions.[4] Hence, crystallographic orientation of the film and the misorientation among grains within the

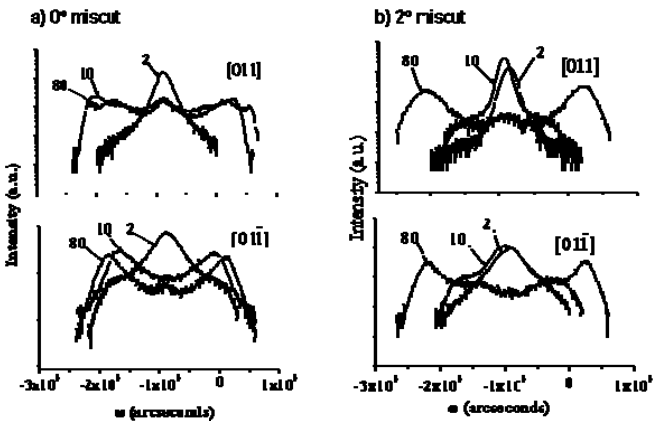

Figure 3A4. InAs (400) rocking curve scans for samples with film thickness of 1.4 μm with growth V/III ratio (indicated by arrows) as parameter (constant growth temperature of 700°C): samples with a) non-miscut substrate, b) with 2° miscut substrates.

InAs film is strongly affected by both the growth temperature and substrate miscut.

AFM images of films grown for 20 minutes (~1.4 thick) are shown in Figure 3A3. They show that the film morphology also is affected by the growth temperature and by the substrate miscut. Table 3A1 lists root mean square (RMS) roughness values determined from the AFM data. The RMS roughness increases with the growth temperature. At 600°C and 700°C constant temperature, it is smaller for growths on 2° miscut substrates than it is on 0° miscut substrates. These film show a rough, crosshatch surface morphology with an RMS roughness of >100 nm (observed in large area AFM scans not shown in the figure). At 500°C on the films are equally smooth on both substrates with an RMS roughness of ~10 nm. The relatively smooth surface is interrupted, however, by 70-100 nm deep pits of ~0.5 μm diameter at a spacing of ~ 2-4 μm. The growth morphology at 500°C appears, in regions, similar to that associated with a spiral growth mode at screw-dislocations that has been observed previously observed in MOVPE InAs grown on GaAs at 530°C. [5]

Figure 3A4 presents x-ray rocking curves obtained from the (400) InAs peak as a function of V/III ratio at constant growth temperature of 700°C for 0° and 2° miscut samples, respectively. For the 0° miscut sample, a single peak appears for the lowest V/III ratio of 2, whereas multiple peaks are observed at higher V/III ratios of 10 and 80 in both the scan directions. For the 2° miscut sample, a single rocking curve peak exists for the V/III ratios of 2 and 10 in both the scan directions. For the samples grown at V/III ratio 10, scans obtained along $[01\bar{1}]$ show broad, low intensity shoulders. At a V/III ratio of 80, multiple peaks are present in both the scan directions for both 0° and 2° miscut samples. Thus, singular orientation is correlated with a lower V/III ratio and a miscut substrate. Table 3A2 summarizes the peak splitting between multiple peaks and the FWHMs of individual single peaks for the x-ray rocking curve scans.

Table 3A1. RMS roughness for 1.4 μm thick InAs film and island number density for 12 second of InAs deposition: effect of growth temperature and V/III ratio.

T(°C)	V/III ratio	Miscut	Island number density, 12 s (x $10^8 cm^{-2}$)	RMS roughness (nm)
500	80	0° 2	40 50	7 12
600	80	0° 2°	~0.1 ~0.4	116 59
700	80	0° 2°	0.430 15.000	141 118
700	10	0° 2°	0.015 0.030	164 153
700	2	0° 2°	0.430 0.330	39 30

The remaining studies performed in this project used growth conditions that favor low nucleation rates (700°C; V/III ratio of 80) in order to investigate the origin of tilt and means to inhibit it. The microstructure in Figure 3A1 serves as a base line for these studies. This part of the research addressed two general issues: (1) understanding the origin of the tilt microstructure by exploring a correlation between the size and shape of the InAs deposit in the island stage of growth and tilt within individual islands; and (2) the use of lateral epitaxial overgrowth as an alternative method to control film microstructures in which behavior during the island nucleation and growth is controlled not by the chemical and kinetic environment, but physical constraints imposed by the masked substrate. The complementary nature of chemical and physical methods for controlling growth topography became a threading theme of this work as it progressed.

Table 3A2. Peak splitting and FWHM of x-ray rocking curve peaks for non-miscut and 2° miscut samples: effect of film thickness

Thickness (μm)	Substrate	Scan Direction	# of peaks	FWHM (arcs)	Peak Splitting (°)
1	0° miscut	$[01\bar{1}]$	2	---	3.6°
		$[011]$	3	---	8.1°
	2° miscut	$[01\bar{1}]$	4	---	6.8°
		$[011]$	3	---	6.4°
2	0° miscut	$[01\bar{1}]$	4	---	6.3°
		$[011]$	3	---	6.8°
	2° miscut	$[01\bar{1}]$	4	---	5.8°
		$[011]$	3	---	6.3°
3	0° miscut	$[01\bar{1}]$	4	---	6.1°
		$[011]$	3	---	6.0°
	2° miscut	$[01\bar{1}]$	2	---	4.3°
		$[011]$	1	3100	---
10	0° miscut	$[01\bar{1}]$	2	---	3.4°
		$[011]$	3	---	6.8°
	2° miscut	$[01\bar{1}]$	1	9300	---
		$[011]$	1	2275	---

3B. Importance of Window Width in Lateral Epitaxial Overgrowth

In other large-lattice mismatched materials systems, most notably GaN on SiC and sapphire, application of the lateral epitaxial overgrowth technique (LEO) has lead to substantial reduction in the threading dislocation and other defect density in the epitaxial film.[6,7] Fig. 3B1 schematically illustrates the basic concept of LEO. A LEO substrate consists of a wafer on which an amorphous mask material has been deposited, into which a pattern is etched to expose the original substrate surface in 'windows.' The pattern commonly consists of holes, or, as in the present case, stripes oriented along a favorable crystallographic direction. The epi-layer nucleates in and initially grows to fill the windows. This material typically has the epitaxial orientation and defect density characteristic of growth on an unmodified substrate for the materials system of interest. As the LEO deposit grows out over the amorphous mask, however, it is no longer constrained to match the substrate lattice parameter. Significant defect density reduction is realized over the volume of the film, often in direct proportion to the mask to window surface area. The example of InAs/GaAs shown in Fig. 3B1 demonstrates that surface roughness is a possible cost of the improved crystal quality obtained via the LEO process. Whether the InAs surface can be planarized through optimization of growth conditions, introduction of a surfactant during growth, or post growth planarization is a topic for further study. Figure 3B1 shows cross-sectional secondary-electron SEM micrographs of as-cleaved LEO samples with 0.8μm wide windows. The generally triangular cross-section of the "bars" of growth above the window is typical for windows oriented along GaAs $[01\bar{1}]$. The growth has proceeded to coalescence of neighboring bars, resulting in a 1-3 μm thick continuous film of InAs. The coalescence boundary is void free. The film surface is rough on the scale of micrometers The

bar sidewalls are the {111}A slow-growth planes of InAs. As the window opening increased from 2 to 5 μm, the surface morphology above each window evolved into a double-ridge structure with the same {111}A type sidewalls bounding each ridge of material. In a parallel study multiple ridges formed above windows with yet wider openings of 5-10μm.[10]

A portion of this research program focused on assessing the utility of the LEO approach for improvement in the crystal quality and microstructure in the InAs/GaAs system as a model for other 6.1Å materials on semi-insulating GaAs substrates. Two improvements in InAs film quality were observed for films grown on LEO substrates compared to those grown on unmasked substrates using the same growth conditions. First, the treading dislocation density in the LEO InAs material decreased by more than an order of magnitude and in some cases as much as three orders when compared to the conventional film. Secondly, constituting perhaps the most significant result of this part of the work, a critical dependence of the development of microstructure in the film on the window dimension was observed in this study. The crystal tilt observed in growths on unmasked substrates was ameliorated in films grown on substrates with sum-micron windows, and the threading dislocation microstructure was altered, not just reduced in density. These dramatic changes in film microstructure suggest that the mechanism of defect introduction into the growing film also changes as the windows become submicron in width.

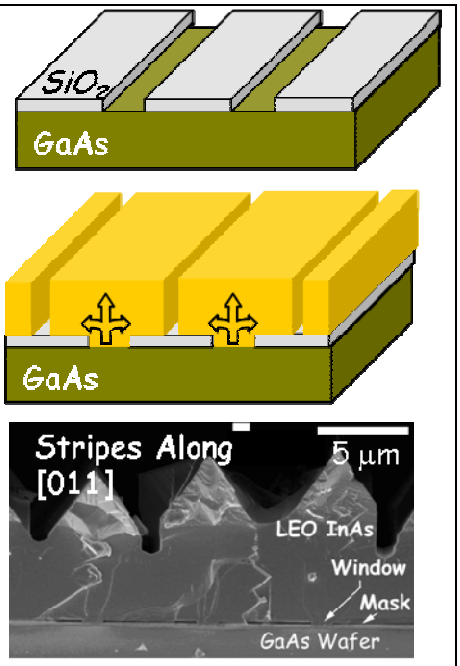

Figure 3B1: Illustration of the LEO method and growth produced on 5 micron wide windows

Double-crystal x-ray rocking curves were used to characterize the general crystal quality as a function of the width of the window. The rocking curves in Figure 3B2 show a dependence of InAs orientation and mosaic spread on both window width and crystallographic direction. The rocking curve geometry for Figure 3B2 probed crystal orientation and (400) mosaic spread perpendicular (parallel) to the long axis of the window. As described in section 3A, the InAs grown at 700°C on the infinite-window-width (i.e. unpatterned) substrate is composed of domains tilted in to one of six preferred directions relative to the GaAs. The rocking curves in Figure 3B2 show that as the mask is introduced and further as the windows become narrower, the angles of misorientation in scans perpendicular to the long axis of stripes decrease until a single orientation, in registry with the (100) GaAs, is observed for the 0.8 μm wide windows. Along the stripe axis, a single orientation, aligned with the GaAs substrate, was observed for all LEO samples. Figure 3B3 provides a schematic illustration of the development of the tilted InAs characteristics from wafers to wide windows to submicron windows. In addition the full width at half maximum (FWHM) of all of the peaks in both directions decreases with decreasing window width, indicating a concomitant general improvement in crystal quality.

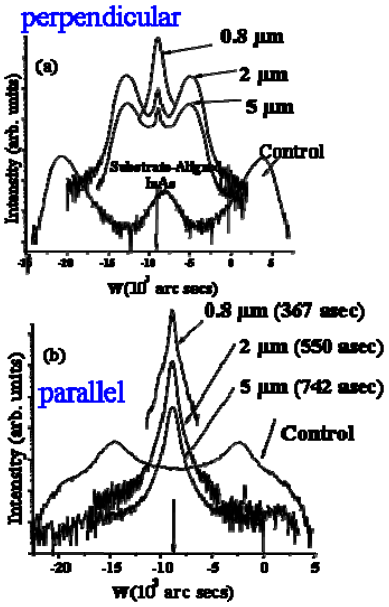

Fig 3B2: [004] x-ray rocking curves obtained rocking parallel and perpendicular to the [011] direction in the GaAs as a function of window width.

Cross-sectional TEM of InAs films grown on substrates with infinitely-, 5 μm- and 0.8 μm-wide windows revealed microstructures and microstructural changes that were both consistent with the x-ray rocking curves and indicative of basic changes in microstructural development with narrowing window width. Two features that dominate the microstructure of InAs grown on the infinite-window substrate are shown in Figure 3B4. They are: (a) low-angle grain boundaries that thread the film from substrate to surface and separate grains, each of which are misoriented by ~3° relative to the substrate, and (b) sets of dislocations that appear at many locations throughout the film. The grain size near the substrate is ~1 μm. Estimates of the dislocation density as a function of distance from the substrate are given in Table 3B1.

A bimodal microstructure was observed in the films grown on LEO substrates with 2 and 5 μm wide windows as shown in the TEM micrograph of Fig. 3B4 of a 5 μm wide window. The microstructure in the material above the window was qualitatively the same as that observed throughout the sample grown on maskless wafers. The material above each of the nine 5 μm-wide windows examined contained at least two grains misoriented by a few degrees with respect to each other. In contrast, no new grains, and thus no new low-angle grain boundaries, formed in the overgrown material above the mask. Thus, defect reduction roughly in proportion to the mask-to-window surface area (Table 3B1) is realized in this film, consistent with the sharpening of the x-ray rocking curve peaks. The TEM micrograph in Figure 3B5 shows the defect microstructure that occur in both the vicinity of the window and in the entire film when the window width is

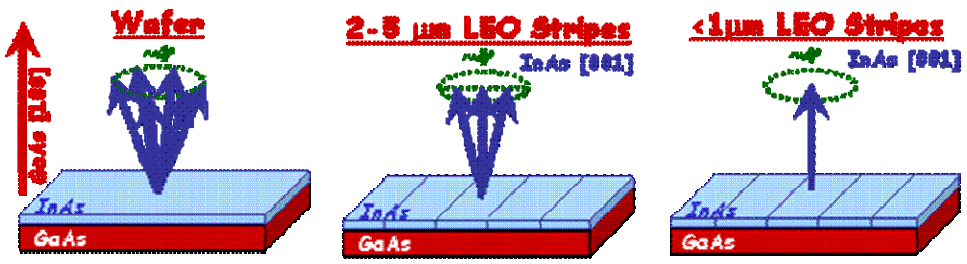

Figure 3B3: Schematic illustration of the preferred tilts observed on wafers, in LEO growths, and in LEO growths with submicron wide windows.

reduced further to 0.8 μm. First, a single low-angle grain boundary bisected almost every window of the seventeen observed. In contrast to growth on the other substrates, however, the misorientation angle of each boundary above the 0.8 μm wide windows decreased with distance from the substrate until the boundary effectively terminated ~0.75 μm into the film. Second, the material directly above the exposed GaAs is heavily populated with dislocations. However, these dislocations are confined to the volume just above the window and within about 0.25 μm from the GaAs surface. Elsewhere in the film the dislocation density is reduced by more than two orders of magnitude (Table 3B1). Third, there is evidence that dislocations in the window region are induced to lie parallel to the substrate as the film thickens, rather than thread to the film surface. Fourth, it appears possible for the plane of intersection of two neighboring overgrowths to be defect free.

TABLE 3B1. Estimated dislocation density as a function of distance from the GaAs substrate.

Distance from the InAs/GaAs interface (μm)	0.8μm window (cm^{-2})	5μm window (cm^{-2})	Infinite (cm^{-2})
Within 0.15	$> 10^{11}$	$> 10^{11}$	$>10^{11}$
0.15 - 3	7×10^{8}	8×10^{9}	1×10^{10}
> 3	9×10^{6}	1×10^{9}	Exceeds film thickness

The general reduction in defect density, Table 3B1, is consistent with the reduction in x-ray line width with decreasing window width. Similarly, the termination of the low-angle grain boundary in the first three-quarter micrometers of growth is consistent with the loss of multiple peaks in the x-ray rocking curves. At the time these results were published, we had suggested that these improvements resulted from changes in microstructure that were driven by factors in the growing film rather than at nucleation[8] and speculated that these factors most likely were stresses induced by the presence of the mask edges when their dimensions approached that of the window opening. The subsequent studies of tilt domains within islands described in sections 3D indicate that it is the size of the islands at coalescence and the effect of the LEO substrate on controlling that size that leads to singular orientation, not mask-induced stresses. The x-ray and TEM studies showed that defect reduction is realized upon application of the LEO technique to the InAs/GaAs system. More importantly, the basic character of the microstructure changes in a way that accelerates defect reduction when the window width is less than ~1 μm. The BEKP experiments described in sections 3D-E suggested a possible mechanism for

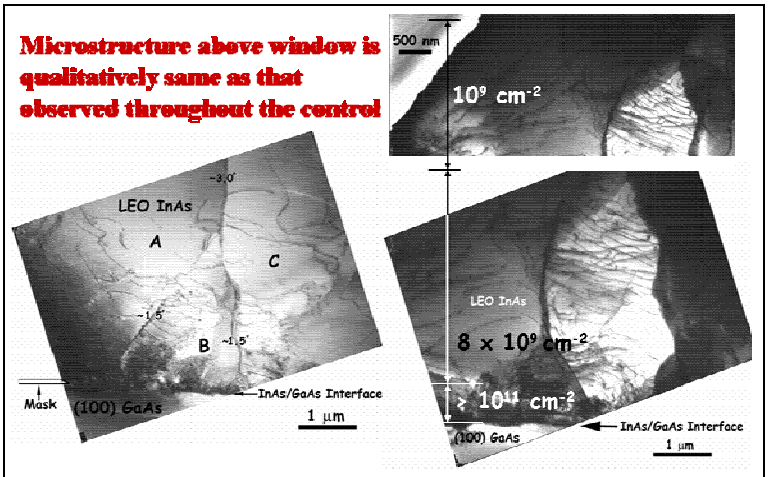

Figure 3B4: Microstructure observed in films grown on maskless wafers and above the windows on LEO samples with windows 2 μm and 5 μm wide (shown here).

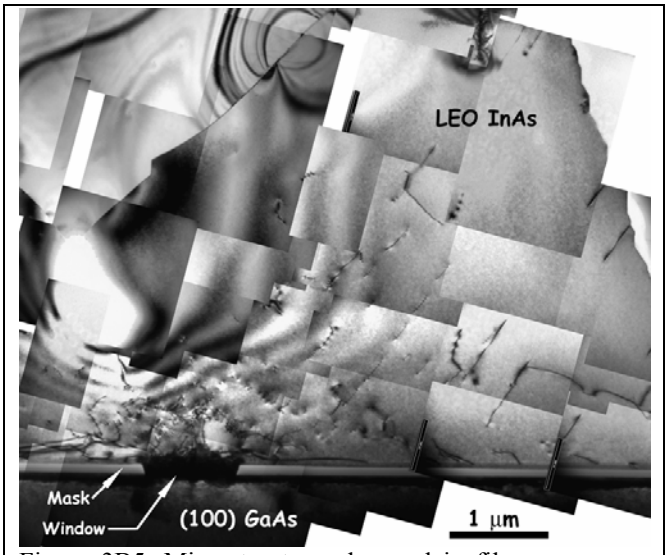

Figure 3B5. Microstructure observed in films grown on 0.8 μm wide windows.

this transition.

The orientation images in Figs. 3A1 and 3B6-7 show the evolution from the tilted-grain microstructure characteristic of the InAs films grown on un-patterned substrates (Figure 3A1) to a singular orientation as the LEO window width is reduced to below 1 μm (Fig 3B7). Fig. 3A1, from a film on a mask-free wafer, shows columnar grains with mean linear intercept diameters on the order of a few micrometers. It suggests that the tilt is established at the substrate/ film interface and propagates directly through the film with little for evolution of the distribution of tilted material with thickness. The orientation image in Fig. 3B6 was obtained from a sample with 5 μm wide windows and a 1:1 ratio of exposed GaAs to SiO_2 on the substrate. Three features distinguish this image from that obtained for the maskless wafer, Fig. 3A1. First, the magnitude of the InAs tilt relative to the GaAs substrate has decreased from ~4° for most grains on the maskless wafer (clearly evident when the GaAs is used as the reference orientation and from x-ray rocking curves, but not shown in Figure 3A1) to less than 2° in the bulk of the LEO material. Second, the angle of misorientation between the GaAs and the InAs in and directly above the centers of the windows is greater (~2-4°) than it is both near and above the edges of the window and over the mask (≤2°). And third, the domains with the larger misorientations near the center of the window do not propagate through to the film surface, rather the less-misoriented material that nucleated at the window edges appears to grow over both the mask and the material in the center of the window.

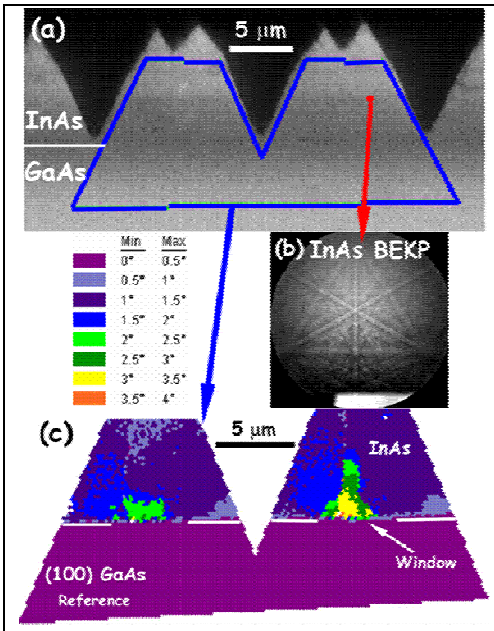

Figure 3B6: BEKP orientation image obtained from a sample with 5 μm wide windows and a 1:1 ratio of exposed GaAs to SiO_2 at the surface of the substrate.

Fig. 3B7 shows the orientation image of a cross-section of LEO InAs grown on a substrate with 0.8 μm wide windows and an approximately 1:10 ratio of exposed GaAs to SiO_2 at the surface of the substrate. The InAs in the window, above the window, and above the mask all is oriented within 0.5° of the GaAs reference orientation. Singular orientation was indicated by x-ray rocking curves from this sample as well. The changes in misorientation angle with window width measured in the BEKP experiments are consistent with the mosaic spread deduced from the x-ray rocking curves for all samples examined. Thus, the BEKP results for individual bars of InAs are believed to be representative of each bar even though they are measured, reproducibly, over a relatively small volume of the sample (approximately 10 windows per sample, of which two are shown in the figures). They indicate that the misorientation of the material close to the window edges is small relative to that near the window centers and, thus, that the better alignment achieved as the window width is decrease is induced by minimizing the area associated with the "window center." These results demonstrate the power of combining BEKP measurements of local orientation with broader beam x-ray diffraction measurements for understanding the microstructure of the film and its origin. They also motivated the study of orientation at the island stage of growth for the LEO materials that is described in section 3E.

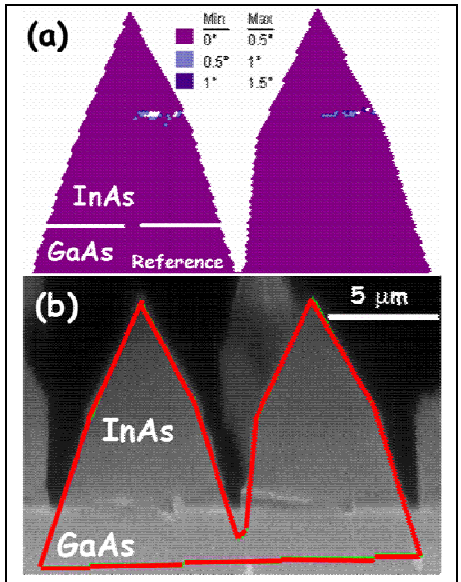

Figure 3B7: BEKP orientation image obtained from a sample with 0.8 μm wide.

3C. Island Size and Shape Distribution Studies

The InAs/GaAs system presents the opportunity to observe and understand transitions from pseudomorphic quantum dot growth to strain-relaxed island growth to eventual film growth and the microstructure that results. The characteristics of pseudomorphic growth have been reported on in some depth. The quality and defect microstructure of films also have been studied, albeit to a lesser degree. A comprehensive understanding of the mechanisms of strain relaxation, which can depend on both growth temperature and growth chemistry, and the defect microstructures they induce is desired. This part of the work investigated the effect of growth temperature and V/III ratio on the evolution of the film morphology, orientation, and microstructure from small island to large island to coalesced film.

AFM amplitude (height derivative) images of the island morphology in uncoalesced films grown for 12 seconds, which corresponds to a nominal InAs layer thickness of 10 nm, are shown in Figure 3C1a and 3C1b for 0° and 2° miscut samples, respectively. An estimate of the total island density was obtained from the 10x10 μm^2 scan area. This scan range measures the highest island-number density since the majority of the islands are much less than 1 μm^2. An estimate of the total island density after 12 seconds of growth obtained from such scans is presented in Table 3C1 for a variety of growth conditions. The island number density decreases with increasing temperature for both 0° and 2° miscut samples. In general, the island density (~10^7 to ~10^9 cm^{-2}) is higher for the growth on the 2° miscut substrates., For the growth at 600°C on the 2° miscut substrate, the InAs nucleation appears to occur along the step edges, hence the island lateral size in the direction perpendicular to the steps is limited by the terrace width. The InAs

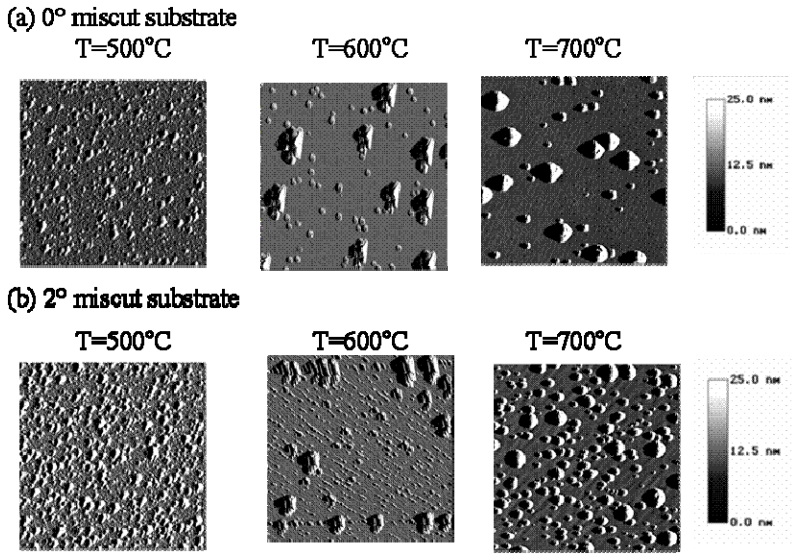

Figure 3C1. Atomic Force Micrographs of samples grown of 0 and 2° miscut substrates.

island size distribution is multi-modal for all the growths periods studied over the range of 4 seconds to 180 seconds. For a growth temperature of 700°C and a V/III ratio 80, the islands coalesce after about 3 minutes of growth which corresponds to nominal thickness of 210 nm with a typical lateral island size of ~3 μm and a height of 300 nm.

AFM scans on samples grown for 12 seconds 700 °C and V/III ratios of 2, 10 and 80 (not shown) indicate that the morphology of islands is not affected to a measurable extent by V/III ratio variations in this range. The island footprints are diamond-shaped with largest island size of ~1 μm and they appear to have a multi-modal size distribution (Figure 3C3), which was determined quantitatively for only the growth at 700°C on 0° miscut substrate. Table 3C1 also lists the RMS roughness for 1.4 μm-thick films. Growth at the lowest V/III ratio of 2 leads to relatively smooth InAs films with an RMS roughness of ~30 nm. At the higher V/III ratios of 10 and 80 the InAs surface is has an RMS roughness > 100 nm due to the presence of ridges and valleys on the surface. Again, growths on 2° miscut substrates possessed a slightly lower RMS roughness than the 0° miscut substrates.

Table 3C1: Island Morphologies and Lengths investigated.

Island Morphology	Footprint	Shape-Defining Facets	Edge/Surf Morphology	Average Width (μm)	Length/Width Ratio	Height (nm)
Pyramidal	Rectangular	{111}	Smooth	0.22	2	110
Domes	Octagonal	{111}, {011}, (100)	Smooth	1.05	1	200 - 210
Rippled	Diamond	-	Sawtoothed	1 – 11	1.3 – 2	350 - 550

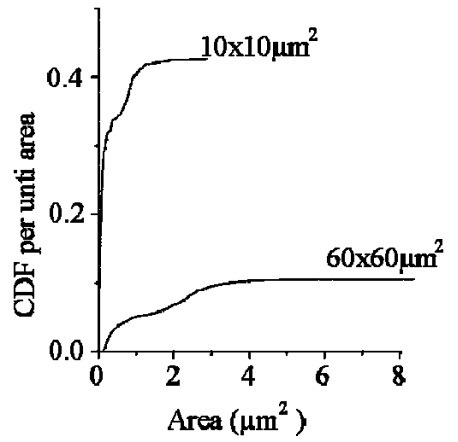

Figure 3C2: Island size CDF for InAs sample grown for 12 seconds at 700°C and V/III ratio 80, for 10 μm and 60 μm scan size.

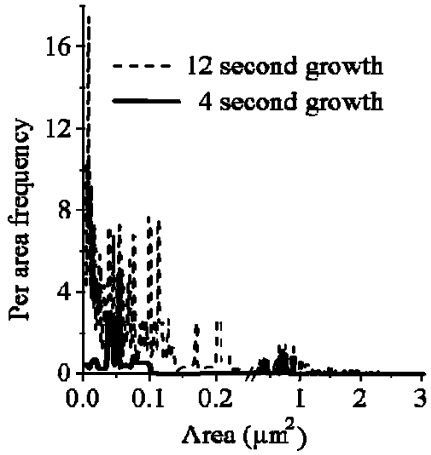

Figure 3C3: Island size frequency distribution function per unit area for InAs sample grown for 12 seconds at 700°C and V/III ratio 80. Note broken x-axis scale.

The samples grown at 700°C and a V/III ratio 80 on 0° miscut substrates for 4 and 12 seconds were used to determine island size distributions. Typical CDFs for the 12-second growth are shown in Figure 3C2 for the 10x10 μm^2 and 60x60 μm^2 sized-scan areas. The higher value of the CDF for the 10x10 μm^2 scans at small values of area reflects the greater resolution of these scans and the high number of measurable small islands. The smaller (10x10 μm^2) scan-size has higher sensitivity to smaller (<0.1 μm^2) islands but cannot accurately determine the areal density of islands of ~2 μm^2 area and larger. The larger (60x60 μm^2 μm) scan-size has a lower cut-off limit at ~ 0.13 μm^2 island size with an improved sensitivity for larger island sizes. Figure 3C3

shows the island size frequency distribution functions (IFD) for the two growth periods formed from the combined data sets. Several distinct island sizes are noted at areas for 12 seconds growth indicating a multi-modal size distribution. There is a large number of islands with an area of about 0.0006 μm^2 as well as larger islands at ~1.9 μm^2. For the 4 seconds growth, again several peaks appear in the island frequency distribution with a higher density at ~0.045 μm^2 and 1.5 μm^2 of island area. The total areal island number density increases from 6.3×10^6 cm^{-2} for 4 seconds growth to 4.3×10^7 cm^{-2} for the 12 seconds growth. The presence of the smallest measurable island size (0.0006 μm^2) for 12 seconds growth and its absence in 4 seconds growth, when combined with the overall rise in island density indicate that multiple waves of island nucleation are occurring during the growth. The ratio of island height to its average lateral size was also measured and was found to vary between 0.08 and 0.1 without any notable trend. Two distinct island shapes are observed for the 12s growth: smaller islands have a pyramidal shape with (111) side facets and larger islands are facetted domes bound by (111) and (110) facets.

Additional IFDs were determined for 12 sec of growth at 700°C and a V/III = 2 for both the 0° and 2° miscut samples The island distributions are similar for both substrates and are dominated by small islands of either $\lesssim$ 0.1 μm^2 or ~0.2 μm^2. This island size distribution contrasts to the multiple island sizes present in the samples grown with a V/III ratio of 80 at the same temperature. As in all the samples grown at temperatures of 600°C or higher, the 2° miscut sample yielded a higher island density. A decrease in growth temperature leads to an increase in the island areal density. The IFD obtained from samples grown at 500° and a V/III=80 after 12 sec of growth time revealed a bimodal distribution with a high density of small islands, < 0.005 μm^2, and a low density of much larger islands at 1-3μm^2. An AlAs 2nm underlayer had a significant effect on the island size distribution. In contrast to the samples without the AlAs layer, the island distribution is strongly bimodal with peaks at <0.1μm^2 and ~ 4.5 μm^2. Is this case, during the 12 sec of growth time, there appears to be two primary and distinct nucleation events.

3D. Island Morphology, and the Development of Tilt During the Island Growth on Maskless Wafers

A critical relationship between the evolution of size and morphology of the islands and the establishment of systematically tilted domains within the InAs has been revealed using BEKP-based OIM. The OIM results obtained show clear evidence of dependences of the onset, orientation, and magnitude of tilt within pre-coalesced InAs islands. Islands < 1 μm in width have the same orientation as the GaAs. Those > 2 μm contain domains of material tilted ~4-5° relative to the underlying (100) GaAs substrate in a systematic pattern. The island footprint changes from octagonal to an elongated diamond shape simultaneously.

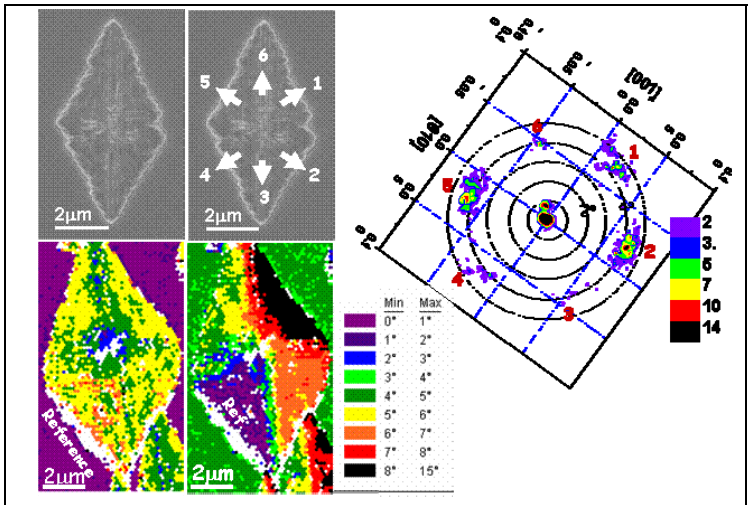

Figure 3D1: SE and OIM images of a diamond shaped InAs island. Left OIM shows orientation relative to GaAs; right show orientation relative to lower left side in InAs. Pole figure was generated from area in the OIM. Arrows in upper right figure indicate direction [100] is tilted in each region.

Figure 3D1 illustrates island shape and the distribution of tilted material that forms within one island when it grow to larger than 2 μm along the axes of the diamond footprint. This distribution of tilted material, its magnitude, direction and location, was repeated from island to island in precisely the same pattern for all islands larger than 2 μm. Every island is separated topographically and crystallographically into six sub-sections. These subsections are delineated by grooves in the surface that run approximately along the <011> directions (gray-scale SEM images in the figure). The orientation images show local orientation with respect to GaAs (image on the left) and with respect to a point in the InAs (right image) for 6.5 μm wide InAs island. The left OIM image shows that all of the InAs is tilted 4-5° with respect to the (100) GaAs. The right hand OIM image and pole figure show that the material within the InAs island is tilted locally and systematically 4-5° about one of 6 rotation axes. Pole figures were constructed for each of the differently colored subsections to deduce the direction of tilt that is indicated by the white arrows in the secondary electron (SE) SEM image. In each sub section, the $[100]_{InAs}$ tilts away from $[100]_{GaAs}$ and toward the edge of the island. The peaks in the pole figure sharpen with increasing island size. The OIM and pole figure for several neighboring, isolated islands of this range in Fig 3D2 show that the pattern of tilt is repeated from island to island. The pole figure obtained from the ~23 islands observed in this scan is largely the same as that obtained from one island and from a much volume of islands by x-ray. It also shows all of the main features of the pole figures

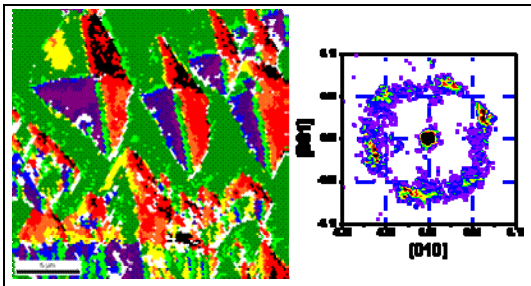

Figure 3D2: OIM image and corresponding pole figure from a group of diamond shaped islands with micron scale dimensions that show the repetition of the pattern of tilt from island to island.

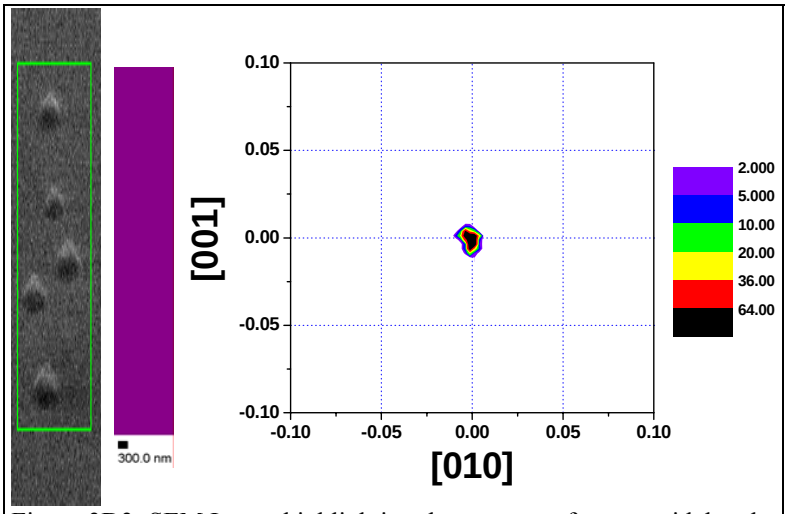

Figure 3D3: SEM Image highlighting the scan area for pyramidal and dome-shaped InAs island sizes) Orientation image of islands in a with respect to GaAs and (c) (100) pole figure from the scan area.

obtained by BEKP and x-ray from thick films grown on mask-free substrates under the same growth conditions (Figure 3A1.)

Figure 3D3 is an orientation image from the pyramidal and dome-shaped islands ≤ 1 μm in width. The area scanned is highlighted in the grey scale SEM image. Islands of both shape morphologies in this size range have the same orientation as the underlying GaAs substrate to at least within the angular resolution of the technique (~ 0.3°). Islands in this size range are 100-200 nm thick, the domes across most of their foot print, but the pyramids only at their apex. A thickness of 100 nm exceeds the depth from which backscattered electrons typically are emitted from materials of medium atomic numbers by about a factor of 3, indicating that the signal obtained from the domes should all have been generated in the InAs. Nevertheless, to assure that the diffraction patterns used to generate these images indeed reflected the orientation of the InAs and not the underlying GaAs, two steps were taken. First for these scans the incident energy of the probing electron beam was reduced from the typical 30 keV to 20 keV. This decrease in electron energy should reduce the interaction depth from which secondary electrons are emitted by a factor of 2. Monte Carlo simulations of the backscattered electron trajectories in the InAs/GaAs system for an InAs thickness of 80 nm were then performed for islands of height 200 nm using the Casino simulation package. These simulations indicated more than 80% of the backscattered electrons emitted traversed only the InAs layer.

These studies show that the multiple tilt microstructure forms during the island growth stage when the islands grow to greater than ~1 μm in width before they coalesce. The tilt microstructure is absent in smaller islands and can be avoided by growing films under conditions that promote copious nucleation and early coalescence at small island size, as is the case for low temperature growths.

3E. Island Size and the Development of Tilt During Island Growth on LEO Substrates

The distribution of and development of tilt in islands grown in LEO substrates was studied with the goal of understanding the origin of the improved crystallographic alignment induced by the LEO process and its dependence on the dimensions of the openings in the LEO substrate mask. The grayscale image in Fig. 3E1 is a secondary-electron SEM micrograph of a 5 μm wide window in a LEO substrate upon which a small volume of InAs has been deposited. The wafer was tilted considerably (70°) relative to the imaging electron beam to the experimental geometry typically used to record BEKPs, resulting in distortion of the island shape. These islands are about 0.3 μm wide parallel to the width of the window with peanut-shaped foot prints, indicating that some, but not all of the islands have coalesced with their neighbors along the length of the stripe. The SEM image clearly reveals the propensity for islands to nucleate preferentially on the GaAs and along the edges of the mask. A few islands are observed in the center of the window. These islands are sparse relative to the density of islands along the mask edge, well isolated from any neighboring islands, generally larger than those found along the edge of the window and often have diamond shaped footprints. This distribution of islands is typical for the early stages of island growth on the 2μm and 5 μm wide windows.

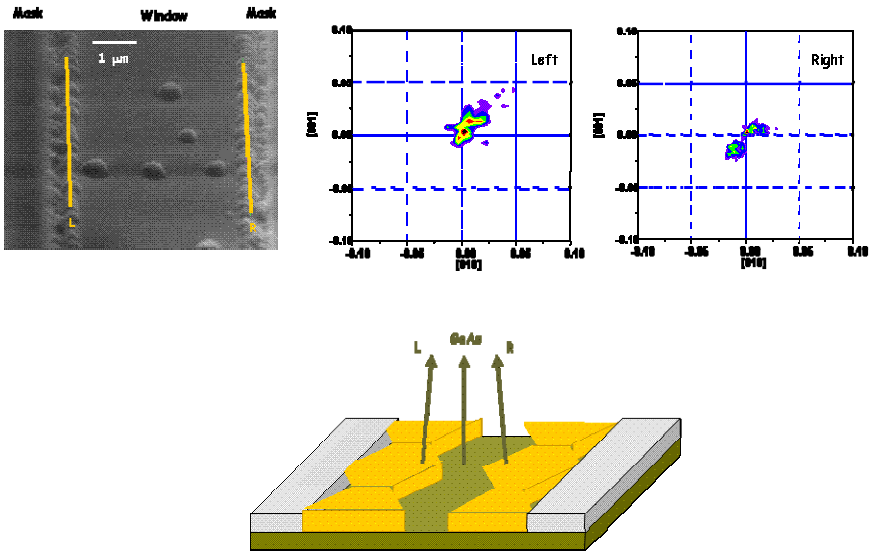

Figure 3E1: Orientations measured during the island stage of growth on LEO substrates. The line scans indicate an orientation of the initial islands at the mask edge which are tilted to the stripe center.

The BEKP-derived pole-figures in Figure 3E1 represent the orientations measured at approximately 250 evenly spaced points along the yellow lines that are superimposed on the SEM image. The pole figure labeled "Left/Right" was obtained from measurements along the line labeled "L/R", respectively.

These pole figures indicate that InAs islands along either side of the window are tilted approximately 0.5° inward away from the window edge about an axis parallel to stripe length, $[01\bar{1}]$. The resultant orientation behavior of the InAs [100] relative to the GaAs [100] and the approximate morphology of the inlands are illustrated schematically at the bottom of Figure 3E1. The $[01\bar{1}]$ rotation axis observed here is not one of the rotation axes observed for the larger isolated islands on the maskless substrates. It does have a common property, however, that appears to be a key to understanding the origin of tilt in these structures: the resultant rotation tilts the InAs toward the one edge of the island whose growth and mechanical behavior is not constrained by intersecting with either the mask edge or a neighboring island. The larger, isolated islands in the growing in the center of the window indicated that center of the window frequently were tilted by much larger angles of misorientation in the range of several degrees.

All of the orientation behavior observed for the islands grown by LEO is consistent with the misorientation distributions observed in the other parts of this project. The tendency for the islands along the mask edge to be better aligned with the GaAs than those in the center of the stripe is consistent the orientation distributions measured in LEO continuous films, figures 3D6 and 3D7, in that the material near the edge of the window is more closely aligned with the GaAs than the material growing in the center of the window. They are also consistent with increase alignment of the InAs as the window width narrows, squeezing out the "central" area on where the more highly misaligned islands are observed to form. They are consistent with the tendency for tilt to set in as the island size increases that was observed for isolated islands on maskless substrates in that the isolated islands near the center of the window are larger in volume and footprint than the islands growing along the edge of the mask. The x-ray pole figure analysis of continuous LEO films grown on windows of various width showed that the successful use of LEO with windows of any width that precludes nucleation on the mask leads to a reduction from six tilt domain orientations to two. This same change from six orientations to two is observed when the tilt microstructure of isolated large islands (Fig 3D1) is compared to that of the island rows that form along the edge of the mask (Fig 3E1). Similarly, the development of just one orientation in the film arises when the window width forces coalescence of the islands in the window width direction before they grow to larger than about a 0.5 μm in width. Together, these results show that the tilt microstructure is established during the island stage of growth and that its character depends on the lateral dimensions of the islands when they intersect their neighbors and coalesce.

4. Discussion

4A. Multimodal Nucleation and Growth

Multi-modal island size distribution is observed in various SK growth mode systems, including InAs/GaAs. The bimodal size distribution of InAs QDs is associated with the growth rate enhancement of dislocated islands relative to coherently strained islands. Very early (island size ~ 30-40 nm) in the growth process of InAs on GaAs, mismatch dislocations form in a fraction of the islands, while the rest remain coherently strained. The higher energy barrier for In-atom attachment onto strained versus unstrained and dislocated InAs islands[9] leads to a difference in their growth rate, which may lead to a bimodal size distribution for the QDs. However, a multi-modal island size distribution is unexpected given the surface diffusion distances involved. In the case of a bimodal distribution, nucleation occurs once but islands can grow at varying rates.[10,11,12] It is clear from this study that nucleation occurs in multiple waves as the InAs deposition continues, resulting in the multi-model island distribution. The effect is particularly pronounced under conditions of high temperature growth. Nucleation is favored in large mismatched systems when the barrier to strain-relief is lowered. Pre-existing dislocations and a decrease in local strain would both result in increased nucleation. The interdiffusion of InAs and GaAs can and does occur at temperature of 700°C over the time scales encountered here. The interdiffusion rate for planar InAs/GaAs surfaces and InAs quantum dots embedded in a GaAs matrix has been studied for the case of strained of initially pseudomorphic layers.[13,14,15] Strain plays a role in altering the diffusion kinetics in thin layers by altering the formation energies for defects, such as vacancies, that underlie the diffusion process. The non-Fickian diffusion that results has been observed in thin layer structures.[16] TEM examination, as in Fig. 3B4, and AFM studies of GaAs wafers from which the InAs has been removed reveal a rough GaAs/InAs with an interfacial width of about 10 nm. The interdiffusion of InAs and GaAs leads to a network of dislocations and a local change of lattice parameter that can lower the strain component of the island nucleation energy. This near surface interdiffusion and defect generation can lead to additional nucleation events and, subsequently, the multi-modal island distribution. The impact of interdiffusion can be mitigated through the inclusion of a buffer layer which impedes interdiffusion. An AlAs layer (1-20nm) inserted below a thin GaAs layer upon which InAs quantum dots were grown resulted in a higher dot density and luminescence efficiency.[17] Park and co-workers attributed the improved performance, in part, to the limited interdiffusion in the growth structure. In the present study, the incorporation of an AlAs layer (2 nm) led to the more bimodal distribution of islands. The extent of interdiffusion therefore plays a primary role in controlling the initial morphology and defect structure of the relaxing and coalescing film.

4B. Tilt, Strain Relaxation, and Island Size at Coalescence

Typical of largely lattice-mismatched epitaxial layers, InAs films on (100) GaAs strain relax by the incorporation of mismatch dislocations during the island stage of growth. Previous studies focused largely on QDs have indicated that this relaxation involves introduction of both 90° ½<011>-type dislocations that form at the island edges and 60° ½<011>-type dislocations that glide in on {111} planes. The burgers vectors of the 90° dislocations all lie in the (100) interfacial plane. Thus, 90° dislocations accommodate

mismatch only. The burgers vectors of the 60° dislocations are inclined to the (100) interfacial plane. These dislocations possess components in the interfacial plane (in plane edge components), perpendicular to the interfacial plane (out of plane edge component) and parallel to the dislocation line (the screw component). The mismatch strains that drive the introduction of 60° dislocations induces only those dislocations with an in-plane component that acts to relax the strain to form. In the most general case, the out-of-plane edge and screw components do not accommodate mismatch strains per se and thus their direction varies randomly among the set of possible choices from dislocation to dislocation. In this case the net screw and out or plane burgers vector content of the mismatch dislocation network is zero and these components of the dislocation burgers vectors do not affect the film microstructure other than the local strain field of the array. If the screw components were biased to lie predominately or exclusively one direction and not the anti-parallel one by an external driving force or kinetic constraint, however, the resulting network of dislocations would act to twist the InAs relative to the GaAs about the common [100] direction, much like a low-angle twist boundary in a homophase material.[18] Similarly, if the out-of-plane-edge components of one set of dislocations were biased by an external driving force or kinetic constraint to line predominately up or down, the resulting network of dislocations would act to tilt the InAs relative to the GaAs about the line direction of the dislocations and an amount proportional to the net burgers vector density pointing "up" or "down," much like a symmetric tilt boundary in a homophase material.

The appearance of a systematic pattern of tilt and the apparent absence of twist in the islands as they grow larger suggests that a driving force or kinetic constraint that biases the out of plane, but not the screw, component of the nucleating 60° dislocations develops as the island grows. A change in the shape of the island appears to accompany this evolution and may be either as a cause or as a result of it. At least two possible causes for such a bias have been discussed in the literature on epitaxy of cubic materials. One proposes that a kinetic constraint is responsible.[19] In this model, miscut of the substrate causes certain of the eight slip systems to be stressed preferentially, thereby favoring formation of the dislocations that belong to the more highly stressed systems. Another model concludes that as the island size increases, the shear stresses that develop near the island surface favor the introduction of 60° dislocations with out of plane edge components that act to tilt the material in the island in such a was so as to accommodate the residual elastic mismatch strain.[20,21] The lack of tilt at smaller island sizes and the development of more refined and larger angle systematic tilt as the island grows larger suggest that the second mechanism may be responsible for the observed tilt. In all cases, the direction of the tilt was, indeed, in the direction predicted for compressively strained islands, as the InAs islands are. Furthermore, the magnitude of the tilt is consistent with a fraction or order half of the dislocations of the mismatch array possessing a biased out-of-plane edge component.

The appearance of tilt in films grown under conditions that favor growth of islands to lateral dimensions in excess of a few micrometers before they coalesce is consistent with this model for the origin of the tilt. An important result of this study is that the means other than chemical environment and kinetic control can be used to promote coalescence at smaller island size, specifically the physical constraint imposed by using an appropriately patterned masked substrate. Integration of a well-designed substrate thus can expand the chemical processing window over which tilt free material can be deposited, thereby expanding possible opportunities for growth of higher quality and perhaps even new materials.

5. Summary

The characteristics of growth of InAs on GaAs are sensitive to precursor chemistry, growth temperature, substrate miscut, and substrate design. The nucleation and strain relaxation steps appear to be somewhat complicated. The dominant of competing mechanisms of growth and strain relaxation depends sensitively on the growth environment and can influence the final quality and microstructure of the film dramatically. Interdiffusion, waves of nucleation and morphology transitions during island growth are characteristic of the growth process. Control of the island size upon coalescence appears to be critical to establishing monolithic orientation in the InAs films grown on GaAs. Two effective routes to achieving this control are suggested by the present results when viewed in the context of the broader project of which they are a part. The first is to control the nucleation and growth kinetics, as could be done by utilizing a low temperature nucleation layer on an unmodified substrate. The second is to incorporate geometric constraints into the substrate, as is done, in conjunction with increasing the nucleation rate at the window edge, in the LEO process.

Bibliography

1. C.R. Bolognesi, J.D. Werking, E.J. Caine, H. Kroemer, and E.L. Hu, IEEE Electron. Device Lett. **14** (1993) 13.
2. O. Hildebrand, W. Kuebart, and M.H. Pilkuhn, Appl. Phys. Lett. **37** (1980), 801.
3 . A. Sasaki, J. Cryst. Growth **160** (1996) 27.
4. "High Resolution X-ray Diffraction and Topography", D. Keith Bowen and Brian K. Tanner (Taylor and Frances, London, 1998).
5. S. P. Watkins, R. Arès, G. Soerensen, W. Zhong, C. A. Tran, J. E. Bryce and C. R. Bolognesi, J. Cryst. Growth **170** (1997) 788.
6. T. S. Zheleva, O. -H. Nam, W. M. Ashmawi, J. D. Griffin, and R. F. Davis, J. Cryst. Growth **222** (2001) 706.
7. M. Hansen, P. Fini, M. Craven, B. Heying, J. S. Speck, and S. P. DenBaars, J. Cryst. Growth **234** (2002) 623.
8. G G. Suryanarayanan, A.A. Khandekar, B.E. Hawkins, T.F. Kuech, S.E. Babcock, Progress in Semiconductors II - Electronic and Optoelectronic Applications, Mater. Res. Soc. Symp. Proc. **744** (2003) 9.
9. K.R. Evans, C.E. Stutz, D.K. Lorance and R.L. Jones, J. Vac. Sci. Technol. **B 7** (1989) 256.
10. G. Saint-Girons, G. Patriarche, A.. Mereuta, I. Sagnes, J. Appl. Phys., **91** (2002) 3859.

11. M.C. Wagener, P.R. Berndt, and J.H. Neethling, Phys. Stat. Sol. (c) **1** (2004) 2343.
12 . S.J. Lee, S.K. Noh, J.W. Choe, and E.K. Kim, J. Crystal. Growth **267** (2004) 405.
13. J.-S. Lee, K. Kudo, Y. Makita, A. Yamada, S. Niki and K. Tananka, Appl. Surf. Science **68** (1993) 251.
14. S.J. Xu, H. Wang, Q. Li, M.H. Xie, X.C. Wang, W.J. Fan, and S.L. Feng, Appl. Phys. Lett. **77** (2000) 2130.
15. M. Tabuchi, M. Araki, and Y. Takeda, Jap. J. Appl. Phys. **41** (2002) 1090.
16. Mariam Gonzolez-Debs, Ph.D. Thesis, Univeristy fo Wisocnsin –Madison, Department of Chemical and Biological Engineering, 2005.
17. Se-Ki Park, J. Tatebayashi, Y. Arakawa, Appl. Phys. Lett., **84** (2004) 1877.
18. G. Suryanarayanan, A.A. Khandekar, T.F. Kuech, S.E. Babcock, Appl. Phys. Lett. 83 (2003) 1977.
19. J.E. Ayers, S.K. Ghandhi, and L.J. Schowalter, J. Cryst. Growth **113** (1991) 430.
20. B.J. Spencer, and J. Tersoff, Appl. Phys. Lett. **77** (1997) 2533.
21. B.J. Spencer, and J. Tersoff, Phys. Rev. **B63** (2001) 205424